Applied Physics A (2020) 126:13
https://doi.org/10.1007/s00339-019-3186-4

Applied Physics A
Materials Science & Processing

Design of metamaterial-based compact and highly sensitive microwave liquid sensor

Sanchita Kayal[1] · Tarakeswar Shaw[1] · Debasis Mitra[1]

Received: 16 October 2019 / Accepted: 26 November 2019 / Published online: 9 December 2019

Abstract
This article presents the design of a compact and highly sensitive mu-negative metamaterial-based microwave sensor for liquid characterization. In the current state-of-the-art development, miniaturization and high sensitivity are the prime concern for designing microwave sensing devices. Hence, the liquid sensor has been developed with the aim to achieve compactness and high sensitivity. This has been realized by introducing a square spiral metamaterial configuration that aids to accomplish notable compactness of the device as well as establishes remarkable sensitivity within a small cross-sectional area. Initially, the sensing characteristic of the device has been verified using the least square method. It is followed by the development of two non-linear equations to calibrate the proposed sensor, which would help to calculate the permittivity of unknown analytes. The high sensitivity and the compactness of the proposed sensor make it an ideal candidate for chemical analysis in various applications.

1 Introduction

In the last few years, the characterization and quantification of the liquid have become essential in various fields such as diagnostics, pharmaceutical procedures, biomedical engineering, industry, agricultural and food safety [1–6]. Usually, most of the liquids are polar in nature and possess some specific electrical properties that carry valuable information about its characteristics. Such electrical properties have a great influence on the performance of microwave devices. When electromagnetic wave interacts with polar liquid materials, distinct electrical properties allow the materials to exhibit different polarization and hence the different orientation of the constituent molecules. Microwave sensors deploy such interaction to exploit the dielectric properties of the liquids for characterization.

Sensors based on electromagnetic approach offer several advantages owing to its fast responsiveness, non-invasive and simple procedure. It necessarily eliminates the use of expensive markers such as fluorescent molecules and gold particles [7] that make sensing approach invasive and costlier. It also eliminates the need for a sophisticated setup and long-term procedure comprising several steps like sample preparation, culture, chemical reactions and measurements [8]. Microwave techniques for liquid characterization can be categorized under the transmission/reflection method and resonant cavity method [9]. The resonant method gets priority due to better sensitivity and accuracy over the narrow bandwidth of operation [10].

In earlier literature, different cavity resonators such as coaxial cavity resonator [11], cylindrical cavity resonator [12], rectangular cavity resonator [13], substrate integrated waveguide resonator [14], have been proposed for the dielectric characterization and concentration measurement of the liquids. Generally, in these resonators, a tube has been incorporated at a maximum electric field region to hold the liquid sample under the experiment. These resonators exhibit a significant change in resonating parameters such as transmission/reflection coefficients, quality factors, and 3-dB bandwidth. However, larger size, complicated configuration and bulky nature of these designs limit their applicability to integrate with the planar IC technology. Afterward, a microfluidic planar resonator has been proposed in [10] to mitigate the previous limitations. Though it provides good sensitivity and compactness, responsivity in peak attenuation is not satisfactory.

✉ Tarakeswar Shaw
tarakeswar.shaw@gmail.com

[1] Department of Electronics and Telecommunication Engineering, Indian Institute of Engineering, Science and Technology, Shibpur, Howrah, West Bengal 711103, India

During the last two decades, electromagnetic metamaterials have been rigorously applied in developing various electromagnetic devices due to their unusual properties. In recent times, metamaterial-based designs have been reported for microfluidic sensing applications [15–17]. Such fluid tunable metamaterials/metasurfaces based sensors have integrated microfluidic channel networks within the architectures to facilitate strong interaction between the electric field and the analytes flowing through the channel. It consequently exhibits high sensitivity. On the contrary, the incorporation of the microfluidic network increases sample volume required for liquid identification. This problem has been mitigated in [6, 18–20] by using unit cell resonating structures proposed for liquid sensing. Usually, these unit cells have been coupled with a microstrip line for the excitation. It enables them to be incorporated into the integrated system. Such structures offer a reasonable shift in resonant frequency using only a few microliters of a liquid sample that is suitable for characterizing expensive samples. However, significant sensitivity along with compactness is still a primary concern in designing a sensor for liquid characterization. Therefore, various research groups are still going on designing miniaturized sensors with high efficiency in terms of sensitivity and selectivity for reliable characterization of liquid.

In this paper, a compact planar sensor using mu negative (MNG) metamaterial has been presented for liquid characterization. The electromagnetic wave propagation has been retarded within the proposed structure over a desired narrow frequency band based on well-known slow wave phenomena [21] by introducing delay. The slow wave effect within the structure has been achieved due to the metamaterial with negative permeability. The slow wave effect consequently strengthens the magnetic coupling which ensures large confinement of electromagnetic waves over the unit cell at resonance. It leads to an increase in the interaction time between the electric field and the liquid to be sensed. Therefore, this feature offers more sensitivity. The overall structure occupies a dimension of $\lambda_0/18 \times \lambda_0/18 \times \lambda_0/153$ (where λ_0 is the free space wavelength), which ensures the compactness and compatibility of the device to IC technology. Also, the spiral resonator has been directly inserted into the microstrip line to create a high perturbation in the resonance due to the analytes. This perturbation leads to an effective disruption in the transmission operation of the microstrip line. The proposed structure is designed in such a way that the electric field remains confined within a small volume. This increases the electric field intensity resulting in a highly sensitive device to the permittivity of the surroundings. The designed sensor provides 0.57% sensitivity by using only 4.92 µL liquid. The proposed compact, highly sensitive metamaterial-based liquid sensor has brought exciting possibilities for liquid characterization.

2 Design and analysis of the sensor

2.1 MNG metamaterial unit cell

Herein, a square spiral metamaterial unit cell structure is considered to design the compact highly sensitive liquid sensor. The designed architecture of the proposed sensor includes a magnetic inclusion which is depicted in Fig. 1a. The main part of the sensor consists of the square spiral resonator which is responsible for magnetic coupling. The resonator is made of a metallic strip line that meandered to reduce the resonator size. It consequently increases effective inductance as well as establishes strong distributed capacitance between the interwinding gaps of the spiral metallic strip. The proposed topology can be modeled with equivalent lumped components [22] illustrated in Fig. 1b. The whole pattern of the proposed sensor is made of copper with thickness 0.035 mm which is designed on the Rogers RO3020 substrate having thickness 0.5 mm, a dielectric constant of 10.2 and low loss tangent 0.0035.

The MTM unit cell structure is excited by parallel electromagnetic plane wave with periodic boundary conditions surrounding the unit cell as shown in Fig. 1a to extract the *S*-parameter characteristics. When the electromagnetic wave is applied parallel to the unit cell structure, magnetic coupling induces current into the spiral metallic part of the structure. Interaction between magnetic inclusion and electromagnetic wave induces a magnetic dipole in the opposite direction of the imposed magnetic field. The simulated transmission and reflection responses of the unit cell are depicted in Fig. 2a. In addition to this, the effective permeability of the spiral metamaterial has been extracted using the Kramers–Kronig retrieval method [23] and manifested in Fig. 2b. All the simulations for the designed structure have been performed using a finite-element method based ANSYS high frequency structure simulator 2019 R2. The effective large

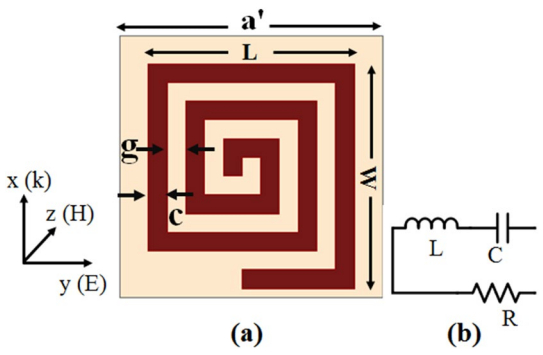

Fig. 1 **a** Unit cell structure of the proposed sensor (where $a'=2.8$ mm, $L=2.2$ mm, $W=2.4$ mm, $g=0.2$ mm, $c=0.2$ mm). **b** Its equivalent lumped circuit

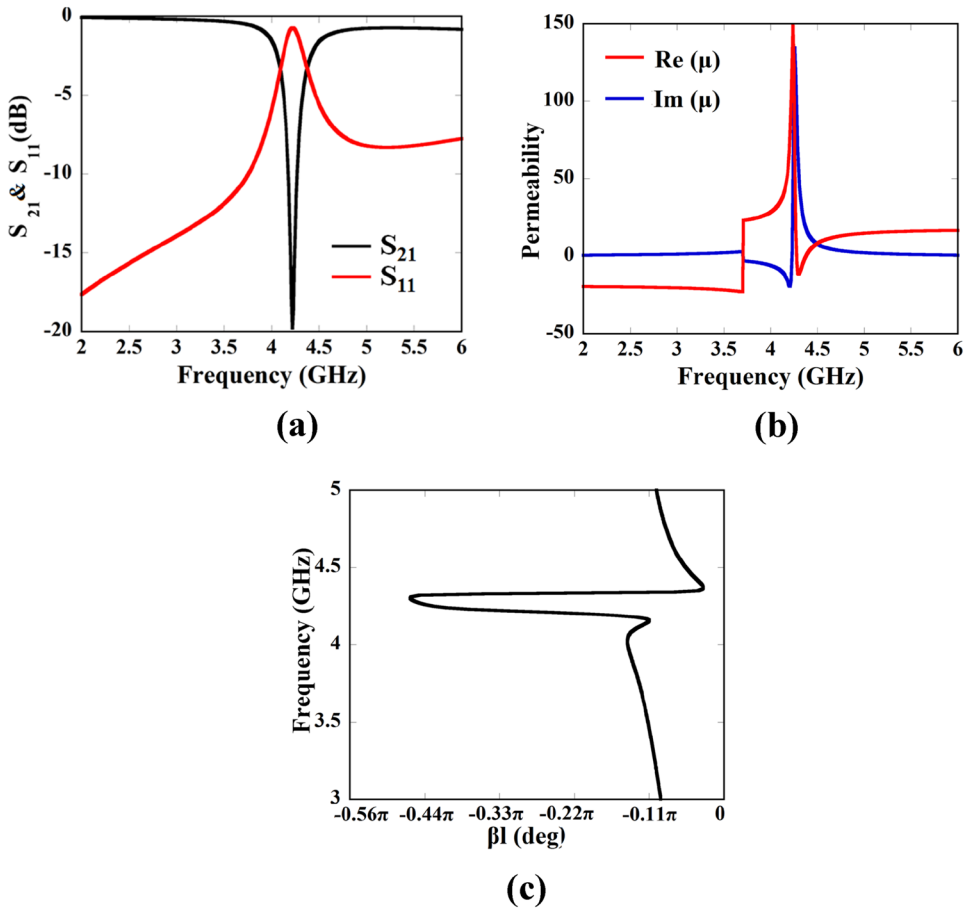

Fig. 2 **a** Simulated *S*-parameters of the MNG unit cell. **b** Extracted permeability of the metamaterial. **c** Dispersion characterization for MNG unit cell

permeability of the unit cell reduces the phase velocity of the wave propagation that has an impact on reducing the guided wavelength which further reduces the size of the structure. Figure 2c establishes the slow wave phenomena of the unit cell that also increases the interaction between the structure and the incident wave. It leads to confine a large electric field within the unit cell. The simulated dispersion diagram has been extracted using the relation

$$\cos(\beta l) = \left(\frac{1 - S_{11}S_{22} + S_{21}S_{12}}{2S_{21}}\right) \quad (1)$$

where β is the phase shift and l is the path length in mm along the direction of propagation. Current flow through the spiral resonator develops a potential difference among the adjacent arms that confine a large electric field at resonance. Spiral resonator offers a large distributed capacitive area leading to considerable change in capacitance due to a small change in environmental permittivity.

2.2 Design of the MNG metamaterial based sensor

In this sub-section, the designed MNG metamaterial structure presented in the previous section is used to design the microwave liquid sensor. Figure 3 illustrates the complete microwave sensor composed of metamaterial resonator connected to 50-ohm microstrip lines at both ends in

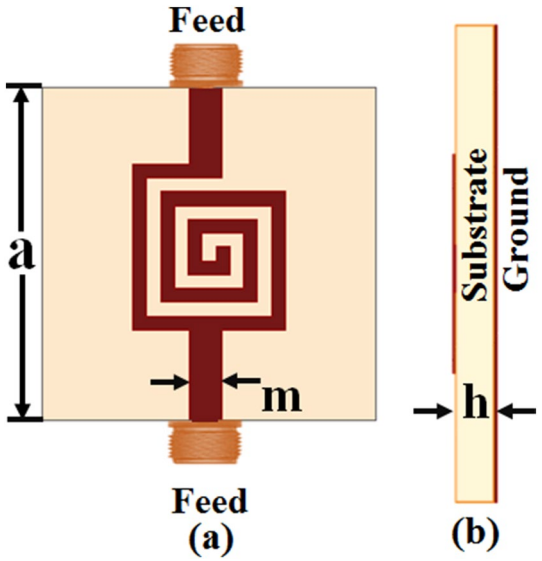

Fig. 3 Schematic diagram of the proposed sensor. **a** Top view. **b** Side view (where $a = 4.8$ mm, $m = 0.47$ mm, $h = 0.5$ mm)

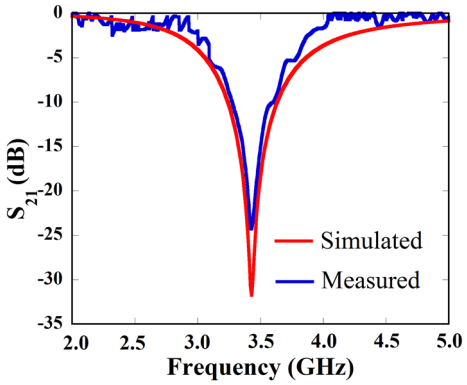

Fig. 4 Simulated and measured transmission characteristics (S_{21}) of the proposed sensor

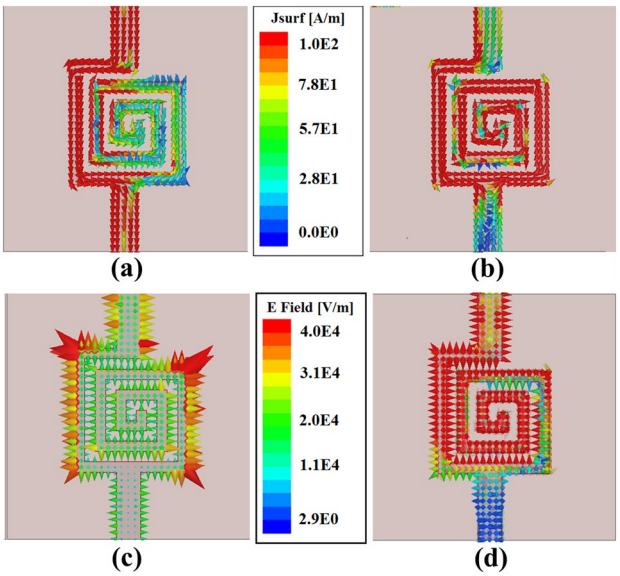

Fig. 5 Current distribution for the designed sensor. **a** At non-resonance. **b** At resonance. *E*-field distribution of the proposed sensor. **c** At non-resonance. **d** At resonance

order to excite it. A metallic ground has been placed on the opposite side of the substrate to guide the wave parallel to it through the substrate from one port to another. Insertion of the microstrip line introduces additional inductance in series with the series lumped circuit contributed to a left shift of the resonant dip from 4.22 GHz indicated in Fig. 2a to 3.43 GHz as shown in Fig. 4. Figure 5 describes the current density and electric field distribution of the proposed structure at non-resonant and resonant conditions. It ensures the confinement of a large electric field within the capacitive gap of the spiral resonator at resonance resulting minimum transmission coefficient at the output. The resonant frequency of the designed resonator can be expressed as

$$f_0 = \frac{1}{2\pi\sqrt{LC}} \tag{2}$$

where L and C are the effective inductance and capacitance of the designed sensor, respectively.

Capacitance C can be approximated by the relation

$$C = \varepsilon_{\text{eff}} C' \tag{3}$$

where C' is considered as the capacitance of the spiral resonator in air and ε_{eff} is the effective dielectric constant due to the substrate, walls of the liquid container placed on the sensor and the liquid sample loaded in the container.

$$\varepsilon_{\text{eff}} = f\left(\varepsilon_{\text{s}}, \varepsilon_{\text{c}}, \varepsilon_{\text{l}}\right) \tag{4}$$

ε_{s} stands for substrate dielectric constant, ε_{c} is the dielectric constant of the container and ε_{l} represents that of the liquid sample.

3 Sensor characteristics and mathematical model

3.1 Sensing principle

This sub-section describes the basic sensing mechanism of the proposed sensor. Equations (2–4) imply that the resonance of the resonator depends on environmental dielectric properties. The sensing mechanism is based on such dependency between the introduction of a polar liquid in the sensing area of it and its resonant perturbation. Dielectric permittivity is the measure of the resistive capability of the material to the generation of the electric field through it. It decides the number of charges required to form a single electric flux through the material. The relative permittivity of a polar liquid can be expressed [24] as

$$\varepsilon(\omega) = \varepsilon'(\omega) + j\varepsilon''(\omega) \tag{5}$$

where real part of the permittivity (ε') is associated with the stored energy within the liquid that is responsible for the resonant frequency shift and the imaginary part signifies the dielectric loss of the liquid which is associated with the peak attenuation and Q-factor of the resonance. Thus, the transmission characteristics of the resonator can provide complete information about the complex permittivity of an unknown liquid.

3.2 Simulation for device calibration

Here the binary mixtures of distilled water and methanol are considered to be the test samples for investigating the sensor characteristics. Though the Eqs. (2) and (3) represent

a complex non-linear interdependency in between resonant frequency and permittivity, initially a set of linear equations has been formed to describe such relation as mentioned in [18], related to the change in complex permittivity by the following matrix equation

$$\begin{bmatrix} \Delta f_0 \\ \Delta|S_{21}| \end{bmatrix} = \begin{bmatrix} m_{11} & m_{12} \\ m_{21} & m_{22} \end{bmatrix} \begin{bmatrix} \Delta\varepsilon' \\ \Delta\varepsilon'' \end{bmatrix} \quad (6)$$

where $\Delta f_0 = f_{0,sam} - f_{0,ref}$, $\Delta|S_{21}| = |S_{21}|_{,sam} - |S_{21}|_{,ref}$, $\Delta\varepsilon' = \varepsilon'_{sam} - \varepsilon'_{ref}$ and $\Delta\varepsilon'' = \varepsilon''_{sam} - \varepsilon''_{ref}$ the subscripts "sam" and "ref" symbolize for the data corresponding to the sample under test and that for the reference liquid. Δ symbol followed by a parameter represents the difference in that parameter for a sample with respect to that for the reference liquid. Here a mixture of 50% water fraction is taken as the reference liquid.

To device calibration, at first complex permittivity for a set of five binary mixtures of water–methanol at 1.5 GHz have been extracted in Table 1 using the relations proposed in [25]. Complex permittivity, mass density and loss tangent of each mixture are inserted in ANSYS HFSS platform and corresponding transmission characteristics of the proposed sensor are simulated for the device calibration. A polydimethylsiloxane (PDMS) well with permittivity 3.24 and loss tangent 0.0014 has been considered around the strong electric field area of the sensor to hold the liquid sample. Figure 6 exhibits a dependency of the resonant frequency with the thickness of the PDMS well for the liquid sample. It shows that the resonant frequency gets shifted to the lower value with the increase of sample volume that related to the thickness of the PDMS well. This is because more the sample volume more the fringing electrical fluxes pass through the liquid [26]. Larger capacitance leads to lower the resonant frequency. However, beyond a certain thickness of 1 mm all fringing electric field gets concentrated to the liquid sample, there is no further impact of it on the resonant frequency alteration. Therefore, a PDMS well of 1mm height is considered to place the liquid sample.

Figure 7a shows the variation of transmission characteristics of the proposed sensor when it is loaded with the

Table 1 Complex permittivity of water–methanol mixture at 1.5 GHz [25] for the different volume fraction of water for the device calibration

Water fraction (%)	ε'	ε''	$\Delta\varepsilon'$	$\Delta\varepsilon''$
10	33.9	10.9	− 22.0	2.0
30	45.3	10.3	− 10.6	1.4
50	55.9	8.9	0	0
70	66.0	7.2	10.1	− 1.7
90	75.7	5.7	19.8	− 3.2

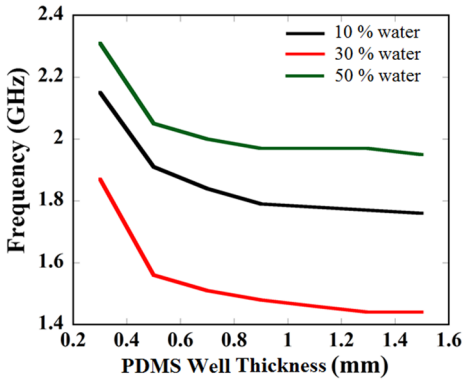

Fig. 6 Effect of the volume of liquid sample (related to the PDMS well thickness) on the resonant frequency for different binary mixture

binary mixtures listed in Table 1. The resonant frequency gets lowered from 1.99 to 1.47 GHz when volume fraction of water in the loaded sample has been changed from 10 to 90% whereas peak attenuation has been increased with the increase of water volume fraction. Figure 7b clearly shows such a pattern of the peak attenuation and the frequency variation of the designed sensor with the different volume fraction of water.

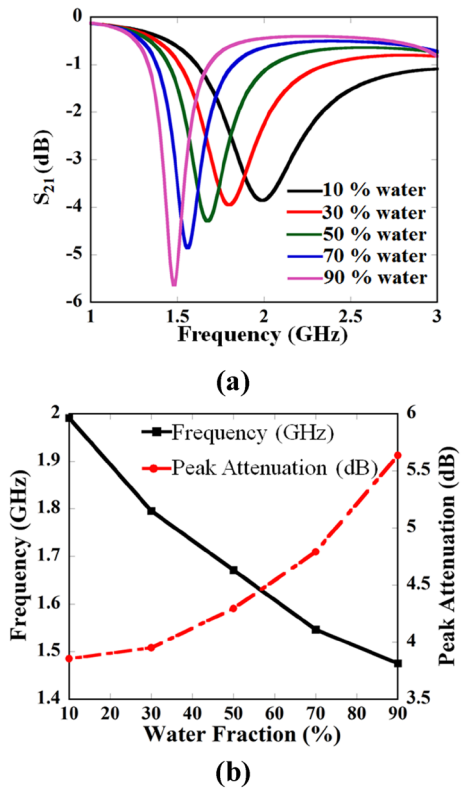

Fig. 7 **a** The simulated transmission response of the water–methanol test samples for calibration of the sensor. **b** Corresponding resonance frequency and peak attenuation

Since the matrix coefficients of Eq. (6) are overdetermined for the above-mentioned dataset, [18] has proposed a least square method to approximate the unknown matrix coefficients. It yields the matrix coefficients in the form of

$$\begin{bmatrix} \Delta f0 \\ \Delta|S_{21}| \end{bmatrix} = \begin{bmatrix} -0.0198 & -0.0578 \\ -0.0374 & -0.6132 \end{bmatrix} \begin{bmatrix} \Delta\varepsilon' \\ \Delta\varepsilon'' \end{bmatrix} \quad (7)$$

Thus, characteristics matrix of the sensor module obtained by doing the inversion of the coefficient matrix in (7) is expressed as

$$\begin{bmatrix} \Delta\varepsilon' \\ \Delta\varepsilon'' \end{bmatrix} = \begin{bmatrix} -61.6078 & 5.8103 \\ 3.7553 & -1.9851 \end{bmatrix} \begin{bmatrix} \Delta f_0 \\ \Delta|S_{21}| \end{bmatrix} \quad (8)$$

This matrix model is helpful to validate the sensing characteristics of the proposed sensor.

3.3 Simulation for device validation

Another set of a binary mixture of water-methanol with water fraction varying from 0 to 100% with a 20% step size is considered to validate the characteristics matrix of the proposed sensor. The complex permittivity related to these mixtures is tabulated in Table 2 from [25]. Figure 8a shows the transmission responses of the sensor for the set of data referred in Table 2.

The corresponding resonant frequencies and the peak attenuations (dB) obtained from Fig. 8b, have been used in Eq. (8) to evaluate the complex permittivity for the device validation and recorded in Table 2. It is observed that the data estimated from our work has good agreement with the extracted data from Ref. [25].

3.4 Modeling for the real part of the complex permittivity

In this subsection, a non-linear relation among complex permittivity of the liquid, resonant frequency, and peak attenuation has also been established. Such mathematical model has been deduced using data in Table 1. As Eqs. (2) and (3) reveal linear relation between the real part of the permittivity (ε')

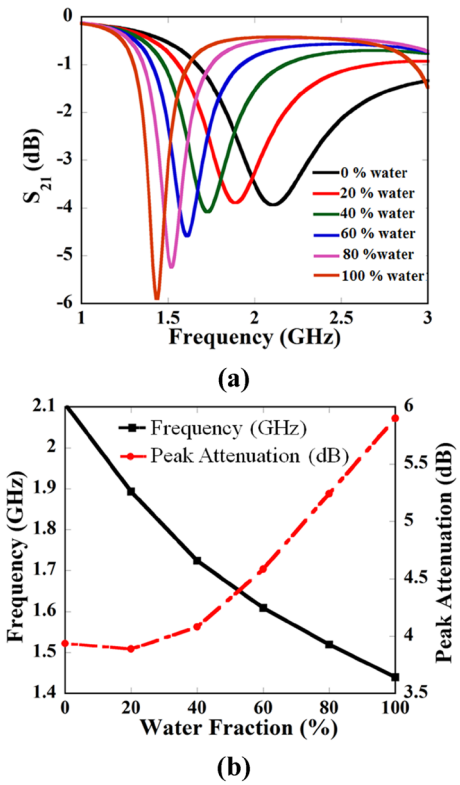

Fig. 8 **a** The simulated transmission response of the water–methanol test samples for validation of the sensor. **b** Corresponding resonance frequency and peak attenuation

and square of the inverse of the resonant frequency (f^{-2}), a linear equation is considered to follow this variation of the resonant frequency to the real permittivity of the liquid. The curve fitting technique has been used to construct the equation in MATLAB. The numerical equation deduced for the real part of the permittivity as a function of the resonant frequency (f) and peak attenuation ($|S_{21,\min}|$ in dB) is expressed as

$$\varepsilon' = 199.3712f^{-2} - 0.0021e^{|S_{21,\min}|} - 16.5948 \quad (9)$$

It is clear from the above equation that the dependency between the real part of the complex permittivity and the

Table 2 Complex permittivity of water–methanol mixture for the different volume fraction of water for the device validation

Water fraction (%)	Estimated from Ref. [25]				Estimated from Eq. (8)	
	ε'	ε''	$\Delta\varepsilon'$	$\Delta\varepsilon''$	ε'	ε''
0	28.0	10.6	−27.9	1.8	27.0	11.2
20	39.6	10.7	−16.3	1.9	39.9	10.5
40	50.7	9.7	−5.2	0.9	51.4	9.5
60	61.0	8.1	5.1	−0.7	61.4	8.0
80	70.9	6.4	15	−2.4	70.7	6.4
100	80.4	5.0	24.5	−3.8	79.5	4.8

peak attenuation (dB) is insignificant compared to that for the resonant frequency and real part of the permittivity. The real part mainly causes a shift in resonant frequency. Figure 9 illustrates the variation of the real permittivity for the set of data referred in Table 1 with the corresponding resonant frequencies extracted from Fig. 7. It demonstrates the fitted curve for the proposed numerical equation (9) as well, which implies that the proposed equation would be an accurate approach to calculate the real part of the permittivity of an unknown liquid.

3.5 Modeling for imaginary part of the complex permittivity

To find out the imaginary part of the permittivity of a liquid, we have again considered the same set of data referred in Table 1 and variation of the imaginary part of the complex permittivity (ε'') of those samples with the peak attenuation ($|S_{21,\min}|$ in dB) is plotted in Fig. 10. Using the curve fitting tool in MATLAB, we have derived an expression,

$$\varepsilon'' = 6.5003 \times 10^4 e^{(2.5-|S_{21,\min}|^2)} + 139.5397|S_{21,\min}|^{-2} + 1.2641 \quad (10)$$

The imaginary part of the permittivity implies the conductive loss of material. It mainly affects the peak attenuation and quality factor of the sensor. With the increase of ε" loss related to the liquid increases which further decreases the peak attenuation.

To validate the proposed equations, the complex permittivity of methanol–water mixture for water fraction varying from 0 to 100% are graphically plotted for both the data tabulated in Table 2 and that obtained from the proposed non-linear mathematical model. Figure 11 exhibits the overlapping of both data which further indicates good accuracy of the proposed numerical model.

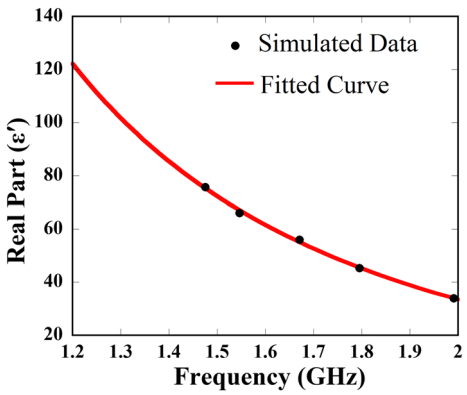

Fig. 9 Characteristics of the real part of the complex permittivity (ε') vs resonant frequency for the designed sensor and its non-linear fitted curve corresponding to the proposed equation

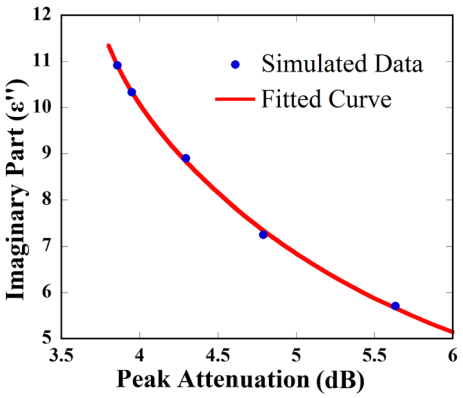

Fig. 10 Characteristics of the imaginary part of the complex permittivity (ε") vs peak attenuation and its fitted curve corresponding to the proposed equation

4 Fabrication and measurement

To validate the performance of the sensor, a prototype of the proposed design has been fabricated using standard printed

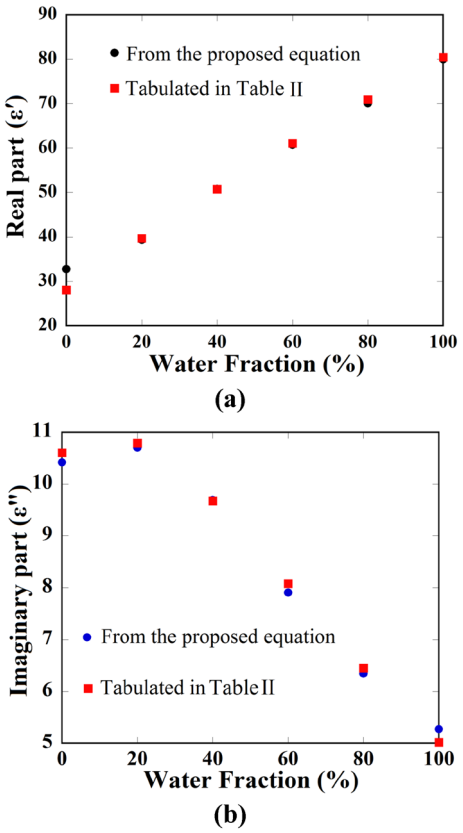

Fig. 11 Comparison between the literature and calculated values of complex permittivity for water–methanol mixtures with water fraction varying from 0 to 100%. **a** Real part of the complex permittivity. **b** Imaginary part of the complex permittivity

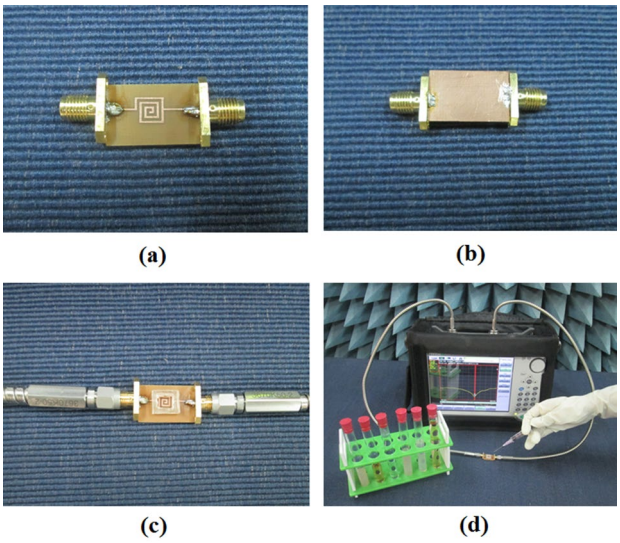

Fig. 12 Fabricated prototype of the proposed sensor module. **a** Top view. **b** Bottom view. **c** Top view with PDMS well placed. **d** The complete measurement setup by the using vector network analyzer

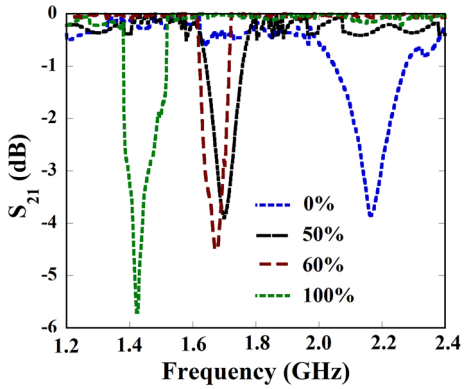

Fig. 13 Measured transmission characteristics of the water–methanol mixtures for different water fractions

circuit board (PCB). The photographs of a fabricated prototype and measurement setup are shown in Fig. 12. A Vector Network Analyzer (Anritsu S820E) is connected at both ends of the feed line through SMA connectors to monitor the responses of the sensor. Samples of water–methanol mixture for different water fractions have been prepared for the experimental validation and the corresponding responses of the sensor are recorded which is illustrated in Fig. 13. It shows a small discrepancy between measured and simulated results, which is usually occurred from the real environmental effect, impedance mismatch as well as the measurement uncertainties and errors, which are not taken into account in the case of simulation.

The electrical size of a sensor can be expressed in terms of resonating wavelength, whereas the sensitivity can be calculated using equation [20].

$$S = \frac{\Delta f_0}{f_0} \times \frac{100}{\Delta \varepsilon} \% \tag{11}$$

where Δf_o and $\Delta \varepsilon$ are the incremental change in the resonant frequency and the permittivity.

A comparative study among the existing microwave sensors in the previous literature and the proposed work has been performed and described in Table 3. It has been observed that our proposed square spiral provides high sensitivity along with compact size compared to Refs. [18–20]. It can also be observed that our proposed work reduces the amount of liquid required for detection than [20]. However, the sensors outlined in [18, 19], required a lesser amount of liquid than our proposed sensor.

5 Conclusion

In this paper, we have designed and demonstrated a compact planar highly sensitive MNG metamaterial-based sensor for accurate liquid characterization. The proposed sensor maintains a small amount of liquid, comparable to the earlier reported sensors while exhibiting higher sensitivity in resonating parameters with respect to the complex permittivity. A mathematical model has been constructed following the least square method to validate the sensor's performance. We have also established and validated two unique non-linear equations that can relate the dielectric properties of the liquid analytes to the proposed sensor's parameters. These equations would be helpful to evaluate the complex permittivity of the unknown liquid. The high sensitivity and

Table 3 Comparison of the proposed MNG metamaterial-based sensor with the other reported metamaterial inspired liquid sensors at microwave frequency

References	Structure	Freq of operation (GHz)	Limit of Detection (μL)	Electrical size	Sensitivity (%)
[18]	SRR	2.01	0.108	$\lambda_0/15$	0.0796
[19]	CSRR	2.00	0.588	$\lambda_0/9$	0.26
[20]	MTM/MS coupler	2.60	5.00	$\lambda_0/2.02$	0.27
Our work	Proposed MNG based sensor	3.43	4.92	$\lambda_0/18$	0.57

compactness of the proposed sensor enhances its integrity factor and usability to industrial and medical applications.

Acknowledgements For research support, T. Shaw acknowledges the Visvesvaraya PhD scheme for Electronics & IT research fellowship award and D. Mitra acknowledges the Visvesvaraya Young Faculty research fellowship award, under MeitY, Govt. of India.

References

1. K.K. Adhikari, N. Kim, I.E.E.E. Trans, Microw. Theory Tech. **64**, 319 (2016)
2. H.J. Lee, J.H. Lee, H.S. Moon, I.S. Jang, J.S. Choi, J.G. Yook, H.I. Jung, Sens. Actuators B Chem. **169**, 26 (2012)
3. K. Grenier, D. Dubuc, P. Poleni, M. Kumemura, H. Toshiyoshi, T. Fujii, H. Fujita, I.E.E.E. Trans, Microw. Theory Tech. **57**, 3246 (2009)
4. H.J. Lee, J.H. Lee, S. Choi, I.S. Jang, J.S. Choi, H.I. Jung, Appl. Phys. Lett. **103**, 053702 (2013)
5. M.P. Abegaonkar, R.N. Karekar, R.C. Aiyer, Rev. Sci. Instrum. **70**, 3145 (1999)
6. V. Rawat, S. Dhobale, S.N. Kale, J. Appl. Phys. **116**, 164106 (2014)
7. K.H. Park, S. Kim, S.M. Yang, H.G. Park, J. Nanosci. Nanotechnol. **9**, 1374 (2009)
8. J.H. Lee, K.S. Hwang, J. Park, K.H. Yoon, D.S. Yoon, T.S. Kim, Biosens. Bioelectron. **20**, 2157 (2005)
9. A.P. Gregory, R.N. Clarke, I.E.E.E. Trans, Dielectr. Electr. Insul. **13**, 727 (2006)
10. T. Chretiennot, D. Dubuc, K. Grenier, I.E.E.E. Trans, Microw. Theory Tech. **61**, 972 (2013)
11. U. Raveendranath, S. Bijukumar, K. Matthew, I.E.E.E. Trans, Instrum. Meas. **49**, 1305 (2000)
12. B. Kapilevich, B. Litvak, IEEE Sensor J. **11**, 2611 (2011)
13. G. Gennarelli, S. Romeo, M. Scarfi, F. Soldovieri, IEEE Sens. J. **13**, 1857 (2013)
14. J.D. Barrera, G.H. Huff, I.E.E.E. Trans, Microw. Theory Tech. **61**, 225 (2013)
15. B. Dong, M. Zhu, H. Fu, M. Tsai, H. Cai, L. Kwong, P. Li, E. Rius, A. Q. Liu, Solid-state sensors, actuators and microsystems conference, (2011), p. 530
16. J.A. Gordon, C.L. Holloway, J. Booth, S. Kim, Y. Wang, J. Baker-Jarvis, D.R. Novotny, Phys. Rev. B **83**, 205130 (2011)
17. R.A. Awang, F.J.T. Lopez, T. Baum, S. Sriram, W.S. Rowe, J. Appl. Phys. **121**, 094506 (2017)
18. W. Withayachumnankul, K. Jaruwongrungsee, A. Tuantranont, C. Fumeaux, D. Abbott, Sens. Actuators A Phys. **189**, 233 (2013)
19. A. Ebrahimi, W. Withayachumnankul, S.A. Sarawi, D. Abbott, IEEE Sens. J. **14**, 1345 (2014)
20. M. Abdolrazzaghi, M. Daneshmand, A.K. Iyer, I.E.E.E. Trans, Microw. Theory Tech. **66**, 1843 (2018)
21. T. Wang, T. Itoh, I.E.E.E. Trans, Microw. Theory Tech. **36**, 1811 (1988)
22. F. Bilotti, A. Toscano, L. Vegni, I.E.E.E. Trans, Antennas Propag. **55**(8), 2258–2267 (2007)
23. Z. Szabo, G. Park, R. Hedge, E. Li, I.E.E.E. Trans, Microw. Theory Tech. **58**, 2646 (2010)
24. H. Sun, T. Tang, G. Du, Int. J. RF Microw. Comput. Aided Eng. **28**, e21258 (2018)
25. J.Z. Bao, M.L. Swicord, C.C. Davis, J. Chem. Phys. **104**, 4441 (1996)
26. R.A. Alahnomi, Z. Zakaria, E. Ruslan, A.A.M. Bahar, S.R.A. Rashid, Microw. Opt. Technol. Lett. **58**, 2106–2110 (2016)